Predicting the influence of combined oxygen and glucose gradients based on scale-down and modelling approaches for the scale-up of penicillin fermentations

Janoska, Agnes; Buijs, Joran; van Gulik, Walter M.

DOI
10.1016/j.procbio.2022.11.006

Publication date
2023

Document Version
Final published version

Published in
Process Biochemistry

Process Biochemistry 124 (2023) 100–112

Contents lists available at ScienceDirect

Process Biochemistry

journal homepage: www.elsevier.com/locate/procbio

Predicting the influence of combined oxygen and glucose gradients based on scale-down and modelling approaches for the scale-up of penicillin fermentations

Agnes Janoska *, Joran Buijs, Walter M. van Gulik

Department of Biotechnology, Delft University of Technology, Delft, Delft 2629HZ, the Netherlands

ARTICLE INFO

Keywords:
Scale-down
Metabolic modelling
Combined gradients
Oxygen and glucose fluctuations
Metabolite pools
Penicillin production

ABSTRACT

In large scale fermentors the cultivated cells are exposed to dynamic changes in the nutrient concentrations due to imperfect mixing. Based on the characterization of these nutrient gradients in space and time, a rational scale down design can be obtained. This study focuses on the combined gradients of dissolved sugar and oxygen concentrations. Based on a recent computational fluid dynamics (CFD) study, firstly a scale-down design was developed. From intracellular metabolite measurements during these scale-down experiments, the metabolic behavior of the cells under highly dynamic conditions was revealed. Under the combined influence of oscillating glucose and oxygen concentrations, the penicillin production declined to 50 % of the value under steady state conditions. This decline was similar as observed during glucose oscillations alone. The influence of oxygen oscillations on the levels of the majority of the intracellular metabolites analyzed was negligible, although these metabolites were strongly affected by the varying oxygen levels under solely oxygen oscillations. Additionally, a metabolic structured kinetic model was developed and validated with data from glucose and oxygen oscillation experiments. This model can be coupled to CFD simulations to obtain an accurate prediction of the performance of industrial strains in space and time in large industrial scale bioreactors.

1. Introduction

To predict scale up effects on the behavior of industrial strains and further improve large scale fermentations, the complexity of heterogeneous concentration profiles in large scale tanks has to be considered. Large scale tanks impose substrate, pH, shear and dissolved oxygen gradients on the microorganisms cultivated due to imperfect mixing. For example, according to a recent computational fluid dynamics (CFD) study of a 300 L multi impeller stirred bioreactor applied for *Corynebacterium*, significant substrate limitation took place in approximately 3/4 of the reactor volume, at locations further from the feeding port, which was located at the top of the reactor, while oxygen limitation took place in ~1/4 of the reactor volume, in zones further away from the sparger, which was located at the bottom of the tank [1]. The cells

Abbreviations: DO, Dissolved oxygen (concentration); CFD, Computational fluid dynamics; MFC, Mass flow controller; qi, biomass specific production/consumption rates of compound i (e.g. Oxygen 'O_2'; Carbon Dioxide 'CO_2', Sugar 's', Penicillin 'p', Biomass 'x'); Ci, concentration of compound i; Xi, intracellular metabolite pool sizegrowth rate; AA, Amino acid; Gly, glycolysis intermediates; Sto, storage compounds; EC, energy charge; TCA, tricarboxylic acid cycle; PPP, Pentose phosphate pathway; PenG, Penicillin-G; ACVS, δ-(L-α-aminoadipoyl)-L-cysteinyl-D-valine syntetase; IPNS, isopenicillin-N synthetase; ACV, δ-(L-α-aminoadipoyl)-L-cysteinyl-D-valine; IPN, isopenicillin N; PAA, Phenylacetic Acid; Ala, Alanine; Gly, Glycine; Val, Valine; Leu, Leucine; Ile, Isoleucine; Pro, Proline; Ser, Serine; Thr, Threonine; Meth, Methionine; Asp, Aspartic acid; Phe, Phenylalanine; Glu., Glutamine.; Lys, Lysine; Asn, Asparagine; Gln, Glutamine; Tyr, Tyrosine; His, Histidine; Cys, Cysteine; Trp, Triptophan; AAA, L- α -amino adipate; Tre, Trehalose; Aratl, Arabitol; Ertl, Erythritol; Mtl, Mannitol; Glc, glucose, G6P, Glucose-6-phosphate; F6P, Fructose-6-phosphate; M6P, Mannose-6-phosphate; FBP, Fructose-1,6-bisphosphate; T6P, Trehalose-6-phosphate; 2PG, 2-phosphoglycerate; 3PG, 3-phosphoglycerate; 6PG, 6-Phosphogluconate; PEP, phosphoenolpyruvate; G3P or GAP, Glyceraldehyde 3-phosphate; DHAP, Dihydroxyacetone phosphate; Pyr, pyruvate, Ac-CoA, acetyl coenzyme A; αKG, α-Ketoglutarate; Succ, succinate; Fum, fumarate; Mal, malate; Cit, citrate; iCit, isocitrate; Rib5P, Ribose-5-phosphate; Ribu5P, ribulose 5-phosphate; E4P, Erythrose 4-phosphate; Xyl5P, xylose 5-phosphate; S7P, Sedoheptulose-7-phosphate; G1P, Glucose-1-phosphate; M1P, Mannitol-1-phosphate; ADP, adenosine diphosphate; AMP, adenosine monophosphate; ATP, adenosine triphosphate; NAD^+, NADH nicotinamide adenine dinucleotide, $NADP^+$, NADPH Nicotinamide adenine dinucleotide phosphate.

* Corresponding author.
E-mail address: A.Janoska@tudelft.nl (A. Janoska).

https://doi.org/10.1016/j.procbio.2022.11.006
Received 11 August 2022; Received in revised form 8 November 2022; Accepted 13 November 2022
Available online 15 November 2022

circulating in the reactor thus experienced these environmental variations as fluctuations in the levels of substrate and oxygen. Such fluctuations influence the behavior and metabolic responses of the cells [2–5] and therefore the productivity of the fermentation.

The heterogeneities in large scale fermentors can be described via an Euler-Lagrange computational fluid dynamics (CFD) approach, resulting in cellular lifelines, which describe the experience of the individual cells regarding nutrient concentration fluctuations in time [6]. Cellular lifelines can be translated to a representative scale-down design, aiming to mimic the gradients taking place in large-scale tanks in lab-scale fermentors, to enable precise monitoring of the metabolic state of the cells under these conditions on a seconds scale. When translating lifelines to a scale down design, metabolic regimes have to be defined first, which are then used to obtain the per-regime residence time distributions and the regime transition patterns, representing the sequence of the regime transitions and their frequencies [6],[1].

To accurately predict the cellular behavior in industrial scale fermentors, both the hydrodynamic conditions in the tank as well as the biological responses to the resulting local concentration changes have to be taken into account [7]. Modelling approaches are thus relying on coupling CFD and biological reaction kinetic models. Lapin et al. have, for the first time, reported modelling approaches where a structured kinetic model was linked to CFD predictions of the dynamically changing extracellular nutrient concentrations. This was achieved by the Euler-Lagrange modelling approach, where the extracellular environment is described as a continuous phase and the cells are regarded as discrete entities [8]. While the hydrodynamics and mixing obtained by CFD models rely on the tank structure, its geometry and the operating conditions, biological reaction kinetic models are based on the cellular behavior, as quantified in scale-down studies using precise omics measurements [9]. Although the most important changes during dynamic conditions rely on metabolite quantifications [9], because those almost immediately reflect the seconds-scale changes in the environment, monitoring the transcriptome or proteome will lead to understanding the biological responses on longer time scales as well. Based on the understanding of biological mechanisms from the scale-down studies, the model structure can be established.

For the construction of biological reaction-kinetic models, several requirements have to be met: these models have to be relatively simple to limit the computational costs, nevertheless, they need to represent the relevant cellular kinetic responses to changes in environmental conditions on a seconds to days scale [10]. A modelling approach in between small black box and large genome-scale models are structured metabolic models [11]. In such models the cellular makeup and some basic control mechanisms are considered. To reduce the complexity of these models [12], the metabolic network is simplified and essential metabolites are lumped into pools. Therefore, several parameters of such models might not have a direct biological meaning, and their values are determined via computational tools such as parameter estimation instead of in vivo or in vitro experiments.

Although in large scale fermentors, fluctuations in the environmental conditions, regarding nutrients, dissolved oxygen, pH, temperature or shear stress might occur simultaneously [13], most scale-down studies have focused on the separate effects of individual nutrient gradients on different microorganisms. The majority of the computational studies related to the hydrodynamic characterization of large scale reactors focus on the influence of sugar gradients [6,14,15], and a minority on oxygen gradients [16–18]. Regarding scale down experiments, also individual glucose [3,19,20], or oxygen fluctuations [5,21,22] have been considered most commonly. Only a few hydrodynamic studies [1,23] and a few recent experimental works [24,25] considered multiple gradients. Combining multiple gradients in scale down studies can bring a closer insight into the actual conditions in industrial fermentors.

In a previous Euler-Lagrange CFD study of *Penicillium chrysogenum* fermentations in a 54 m^3 bioreactor only glucose gradients were taken into account [6]. Experimental scale–down studies on the effects of glucose gradients in *P. chrysogenum* have shown that the penicillin production declines severely during fluctuating glucose concentrations [19]. It was investigated whether decreased levels of enzymes of the penicillin biosynthetic pathway were responsible for the decline in production, because it is well known that too high levels of glucose repress expression of the penicillin gene cluster [26]. Although the concentration of one of the main enzymes involved in the pathway, isopenicillin-N synthetase (IPNS) declined, the substrate for this enzyme, δ-(L-α-aminoadipoyl)-L-cysteinyl-D-valine ACV) did not accumulate, which would indicate that the capacity of IPNS was not limiting. Next, also the concentrations of the precursors for ACV synthesis were measured. However, finally it was hypothesized that neither the decrease of the IPNS level nor the supply of precursors but rather the fluctuations in the ATP availability for the synthesis of ACV was the most plausible cause for the reduced penicillin production [27]. Next to proteome and metabolome measurements, also the transcriptome of the cells was monitored during oscillating glucose levels on different time scales and in two different scale-down systems [28]. This study revealed that the transcript levels of the pathway enzymes changed due to the fluctuations, however, a uniform trend could not be observed in the time frame of a fermentation, neither as a general effect of the fluctuations at different time-scales [28].

The influence of oscillating dissolved oxygen levels was investigated previously as well [5,21]. These studies showed that during oscillating oxygen concentrations, the penicillin production declines to values lower than observed at a dissolved oxygen concentration (DO) representing the average of the cycle. While during a steady low DO, a decline in IPNS activity was observed based on metabolite measurements involved in the penicillin pathway, this observation could not be confirmed during oscillating oxygen conditions. Similarly, the precursor amino acid concentrations did not reason the decline in the production. Therefore, the severe decline in the penicillin production under fluctuating DO levels might be due to fluctuations in ATP levels [5].

In this study we focus on a scale down design to capture the combined effects of glucose and oxygen gradients in *Penicillium chrysogenum* fermentations. As a baseline for the scale down, lifelines in terms of glucose and dissolved oxygen concentrations were used, which were obtained via Euler-Lagrange CFD simulations of an industrial stirred bioreactor of 54 m^3 [Peng Wei, manuscript under preparation].

Within our scale down experiments, for the first time we quantified metabolites of the central metabolism, next to nucleotide levels and the intracellular redox state, during fluctuating DO conditions. Similarly, we evaluated the changes in the levels of these metabolites during the combined glucose and oxygen oscillation experiments, carried out in continuously operated bioreactors, in order to understand the metabolic responses.

Next to the experimental scale down studies related to glucose and oxygen gradients, a mathematical model was developed describing the metabolic responses of the cells to these dynamic conditions in terms of combined glucose and oxygen fluctuations. This biological kinetic model could lead to improved predictions of growth and penicillin production in large scale systems under dynamic conditions and when coupled to CFD modelling approaches, will provide leads for further improvements of large-scale penicillin production.

2. Materials and methods

2.1. Strain, culture media, and fermentor setup

A high-yielding penicillin producing strain (DS17690) was used, kindly donated by Centrient Pharmaceuticals (Delft, The Netherlands) as spores grown on rice grains. Inoculation was carried out as described previously, using spores grown on 10.0 g of rice grains. The media compositions for the different cultivations have been described previously [5].

The combined glucose and oxygen oscillation experiments were

carried out in a 7 L stirred tank fermentor with 4 L working volume (Applikon, Delft, The Netherlands). The reactors were stirred at 365 rpm with a magnetically driven 6-bladed Rushton impeller with a diameter of 85 mm. In the experiments, 0.3 bar overpressure was applied and a gas flow rate of 2 L min^{-1} was used. The inlet gas flow was controlled by mass flow controllers (Brooks instrument B.V., The Netherlands) and before entering the reactor it was passed through a sterile membrane filter (Millipore 0.2 μm). The pH, T and DO were continuously measured (pH sensor Mettler Toledo 405-DPAS-SC-K8S) and controlled similarly as described in [5]. The pH was measured with a Mettler Toledo 405-DPAS-SC-K8S sensor and controlled at 6.50 ± 0.05. For the DO measurements two conventional Clark electrodes (AppliSens, Applikon Biotechnology) were used. The reactor setup, antifoam addition (Basildon Chemical Co. Ltd, UK, Foam-clear EscaFerm S), and data logging (DCU3, Sartorius, Germany) resembled previously reported methods [5].

2.2. Bioreactor cultivations

Each chemostat cultivation was preceded by a batch phase. After inoculation of the reactor with spores, the batch phase lasted approximately 60 h. During the batch phase, when the DO dropped close to 0.082 mM, the agitation and airflow (pressured air) were increased gradually, until a final stirrer speed of 365 rpm and gas flow of 2 L min^{-1} were reached. Antifoam addition and pH control were started only when the spores had germinated, at approximately 24 h.

The chemostat phase was started when the DO increased, the pH increased and the carbon dioxide molar fraction in the off-gas decreased indicating that the glucose was depleted. A continuous medium inflow rate of 0.2 L h^{-1} was used and the weight of the fermentor was controlled at 4000 ± 10 g through an automated, discontinuously operated effluent removal valve at the bottom of the reactor, resulting in a dilution rate of 0.050 h^{-1}. The same gas flow rate and stirrer speed were used as during the last phase of the batch cultivation, 365 rpm and 2 L min^{-1}. Additionally, the overpressure in the reactor was increased to 0.3 bar. The DO in the fermentor was always above 0.163 mM by supplying air, and the DO was not controlled.

The oscillation phase was started after approximately 100 h of chemostat operation. Oscillation cycles of 360 s were repetitively applied for a total duration of approximately 100 h, where both the DO in the fermentor and the glucose supply were varied. The glucose and oxygen supply applied was determined such that the obtained regime residence time fractions in the lab scale reactor matched those of the large scale reactor, predicted by CFD simulations (Supplementary material B: experimental design). An MFCS script was used to control the feed and the gas composition in a cyclic manner. Thereby the medium feed was turned on for 36 s at a rate of 2 L h^{-1} and subsequently turned off for 324 s. The DO control was based on changes within the aeration gas composition, which was a mixture of air and N_2. The first mass flow controller supplied air, and the supplied air flow rate was controlled based on the measured DO in the reactor. This gas flow was mixed with a steady N_2 flow at lower pressures before entering to the second mass flow controller, which provided the desired, constant total flow of the air-N_2 gas mixture. At the time the feed was turned on, the setpoint for the DO control was changed to 0.03 mM to initiate a quick decline of the DO. When the DO became below a threshold value of 0.046 mM, the setpoint was changed to 0.272 mM to achieve a quick increase. Finally, the setpoint was changed another time to 0.109 mM after a DO of 0.068 mM was exceeded. Thereby, DO oscillations were achieved between 0 and 0.21 mmol L^{-1}, whereby the DO dropped below 0.03 mM for a period of 16 s in each cycle. After 100 h of oscillations the final oscillation cycles were sampled in ~40 s time intervals for intracellular metabolite analysis. Finally, after the oscillation phase, the reactor was switched back to chemostat mode, while the DO was restored to the original, steady non-limiting values, for a period of another 50 h. The combined oscillation experiments were performed in duplicate, using identical set-ups and operating conditions.

The DO step and oscillation experiments were performed as described previously [5]. Briefly, in the 0.013 mM or 0.009 mM DO step experiments, firstly a steady state was reached at non- limiting DO levels in ~100 h, after which the DO was reduced to 0.013 mM or 0.009 mM for ~100 h in the two different step experiments.During the DO oscillation experiments, after an initial steady state of ~100 h at non-limiting DO levels in oscillation experiment I, a DO oscillation phase was initiated: the DO was fluctuating between limiting and non-limiting values in cycles of 112 and 120 s duration for the oscillation experiments I and II, respectively. In oscillation experiment II, the cells were exposed to higher DO variations and to longer periods of near-zero DO levels. The DO fluctuated between 0 and 0.127 mmol L^{-1} in oscillation I and between 0 and 0.178 mmol L^{-1} in oscillation II, and the DO fell below 0.003 mmol L^{-1} during 11 s in oscillation I, while in oscillation II, during 23 s [5]. The average DO in a cycle and the cycle time were similar for the oscillation experiments A and B, with an average DO of 0.06 mmol L^{-1} after correction with the probe delay.

2.3. Sampling and analytical procedures

Sampling and analysis for biomass dry weight, total organic carbon, penicillin G and phenylacetic acid quantification by HPLC analysis was carried out as described elsewhere [5]. Similarly, the procedure of rapid sampling for intra and extracellular metabolite quantification and the analytical procedures for HPLC, TOC and microscopy has been described previously [5].

The amino acids were analysed by GCMS, as described by de Jonge et al. [19]. During most experiments, the glycolysis, PPP and TCA cycle intermediates glucose, G6P, F6P, M6P, FBP, T6P, 2PG, 3PG, 6PG, PEP, G3P, DHAP, αKG, Succ, Fum, Mal, Cit, iCit, and and Rib5P, Ribu5P, E4P, Xyl5P and S7P were determined using GCMS [29]. The intracellular storage compounds (Tre, Mtl, Ertl) and the extracellular glucose and trehalose were analysed similarly [29]. During the DO step down experiment to 0.013 mmol L^{-1} and the oscillation experiment II, FBP, PEP, Succ, Pyr, G1P, 6PG, M6P, T6P, G3P, M1P were determined by LCMS according to van Dam et al. [30]. In the DO step 0.009 mmol L^{-1} and the oscillation experiment I, the metabolites FBP, M1P, PEP were analysed with the same LCMS methodology as the nucleotides (see below).

Identification and quantification of nucleotides was performed by LCMS, using an ACQUITY UPLC chromatography system (Waters, UK) coupled to a high-resolution Orbitrap mass spectrometer (Q-Exactive Focus, Thermo Fisher Scientific, Germany). For chromatographic separation, a reverse phase (Kinetex C18 column 2.1 × 150 mm, 1.7 μm; Phenomenex, Torrance, CA, USA) [31] was used at room temperature using 50 mM ammonium acetate pH 5.0 as mobile phase A, and 90 % acetonitrile plus 10 % 50 mM ammonium acetate pH 5.0 acid as mobile phase B (v/v). A flow of 250 μL/min was maintained over a solvent composition from 50 % to 75 % B over 4 min, before equilibrating back to the starting conditions [32]. The mass spectrometer was operated in negative ionisation mode (−2.8 kV), where a full scan from 250 to 1000 m/z at a resolution of 70 K, an AGC target of 10^6 and by setting the max injection time to auto. The 13 C metabolite extract, and synthetic standards from each metabolite were used to confirm identify of the compounds. Raw mass spectrometric data were processed by using XCalibur 4.1 (Thermo) and by Matlab 2020b, where the summed peak intensities of the individual metabolite compounds were expressed as intensity ratios to the corresponding internal standard peaks. Quantification was based on an external calibration using synthetic standards [32,33]. During the 0.013 mM DO step and oscillation experiment II, the nucleotides were determined according to Seifar et al. [32].

2.4. Calculations

The reversible reaction catalysed by the enzyme mannitol-1-

phosphate-5- dehydrogenase reaction was used to obtain the cytosolic NADH/NAD^+ ratio, as presented in Eq. (1) [34]. This reaction and the involved metabolites were assumed to be in equilibrium, as the enzyme catalysing this reaction is highly reversible.

$$\frac{NADH}{NAD^+} = \frac{K_{eq} \bullet M1P}{H^+ \bullet F6P} \quad (1)$$

The energy charge (EC) of the cells was also assessed during the fermentations, and was calculated by the following equation

$$EC = \frac{ATP + 0.5ADP}{ATP + ADP + AMP} \quad (2)$$

2.5. Pool model development

To characterize large scale fermentors where both glucose and oxygen gradients take place, a metabolic model was built which reflects the cellular responses to the fluctuating oxygen and sugar concentrations. This model is aimed to be linked with a CFD model predicting the hydrodynamic behavior of the fermentors. These combined models could result in a detailed prediction of the performance of large scale fermentors, where the inhomogeneities resulting from the imperfect mixing are taken into account.

The model was based on a metabolic structured model of Tang et al. [11], with major modification of the structure, stoichiometry and kinetics taking place. These modifications were necessary in order to incorporate the influence of O_2 next to the changes in the feed rate and thereby the dilution rate. Most importantly, the NAD^+ and IPN pool was incorporated in the model, while the PAA and AA pools were eliminated. Five main intracellular metabolite pools were defined, such as the glycolytic intermediates pool, storage pool, IPN, ATP, NAD+ pools. In addition to intracellular pools, extracellular pools, such as residual glucose, penicillin, biomass concentrations were considered. Next to this, variation in the enzyme levels were also taken into account for the enzymes responsible for storage release and penicillin production. The model captures sugar uptake and phosphorylation, which phosphorylated sugar might partition towards biomass growth, penicillin formation or storage compound synthesis, or are burned to CO_2 to form energy (ATP). The glycolysis and TCA cycle reaction was taken into account forming NADH and ATP. Next to glucose, O_2 is taken up by the cells and via the oxydative phosporylation, and NAD^+ is formed from the NADH cofactors. Most reactions in the model require the NAD^+ and/or ATP cofactor.

The detailed structure of this model, including intracellular metabolite pools, extracellular concentrations, variable enzyme levels, and the reactions, stoichiometry, kinetics and the estimated parameters is presented in the Appendix. The model was fitted to the experimental datasets of both intercellular and extracellular pools of the previously published ramp and steady state experiments, in which the dilution rate was varied [11,35], a sugar oscillation experiment [19] and the oxygen step experiments to 0.013 DO and 0.009 mmol L^{-1} DO [5]. In the ramp experiment, the dilution rate of a glucose limited chemostat was gradually decreased from 0.5 to 0.05 h^{-1}, while in the steady state experiments, the dilution rate was ranging between 0.015 and 0.12 h^{-1} [11, 35].

2.6. Model solvers, simulations and parameter estimation

The reaction rates involving kinetic terms and mass balances in the form of a system of differential equations describing the changes in extra- and intracellular metabolite concentrations in time was set up and solved in Matlab 2018b. The parameter estimation and simulations were carried out by the AMIGO2 toolbox with Matlab [36]. The system of differential equations was used with 'cvodes' solver. For the parameter fitting, the enhanced scatter search (eSS) algorithm was used [37,38]. The cost function to be minimized for parameter fitting was defined by a log-likelihood function [39,40], which results in parameter values that give the highest probability to the measured data [41]. The details of the solver, experimental data processing, model equations and estimated values of the parameters are presented in the Appendix.

2.7. Statistical analysis of the fermentation dataset

All fermentation conditions were performed in two independent reactor runs (with the only exception of the 0.025 mmol L^{-1} DO step experiment). The standard deviations of the measurements were calculated (as presented in Figs. 1 and 2). In Figs. 3–5, the average values and standard deviations of the measurements of the duplicate reactor runs are calculated. For the modelling work, averages were created of the duplicate reactor runs and duplicate (or triplicate) measurements of the variables, allowing for better comparison between the different experimental conditions (Figs. 6–12). The significance levels within the metabolite group changes were calculated with a two-tailed paired T-test between the average measurements of the two fermentations at different sampling points, with $p = 0.05$. For the model evaluation, we have calculated the relative deviation of the model prediction value from the measurement points in each experiment at each time point. In order to characterize the average deviations between metabolite groups or experiments, the average of the relative deviations were taken.

3. Results and discussion

3.1. Dissolved oxygen and extracellular glucose concentrations- combined sugar and oxygen oscillations

During the experiments, a glucose limited chemostat phase was maintained for approximately 100 h, whereby a steady state was achieved at non-limiting values (>0.16 mmol L^{-1}). After the chemostat phase, the oscillation phase was initiated and the fluctuations were maintained for approximately 120 h. Afterwards, the DO was increased back to non-limiting values for approximately 50 h, where again a steady state was achieved in terms of oxygen uptake and carbon dioxide production rates.

Fig. 1a shows the DO profile, measured by duplicate sensors in duplicate fermentors on a seconds scale, after correction for the probe delay (calculations shown in [5]). The total time the cells experienced complete oxygen starvation (DO level below to 0.003 mM), was 16 s. In the rest of the cycle, non-limiting DO values (~0.1 mM) were aimed for. At 0.1 mM, no oxygen limitation is expected [5,42]. The overshoot in oxygen concentration to 0.2 mM, at 120 s in the cycle is due to the delayed response of the DO controller. This is not expected to influence the process, because no metabolic differences are expected between a DO of 0.1 and 0.21 mM [5].

Fig. 1b shows the glucose profile during the initial steady states (at 94 h and 105 h in the duplicate experiments) and during the cycle at the end of the fluctuation phase (at 212 and 232 h in the fermentation in the duplicate experiments). During the initial steady state phase, an extracellular glucose concentration of approximately 30–50 μM was observed. In a cycle, the glucose concentration increased to maximum of around 0.25 mM in 36 s, and subsequently, it gradually decreased to the levels observed during the initial steady states between 36 and 220 – 260 s after the start of the cycle. Between 260 and 360 s, the glucose concentration remained stable at values between 0.03 and 0.05 mM.

The maximum glucose concentration reached in our combined sugar and oxygen oscillation experiments was around 0.25 mM, observed after 36 s, at the moment when the feed period was terminated. This maximum concentration was slightly lower than the concentration of 0.35 mM reported in the study of de Jonge et al., who applied an identical glucose oscillation regime [19]. This might have been caused by the longer mixing time in the reactor during our experiments, due to the slower mixing at a stirrer speed of 365 rpm compared to the study of

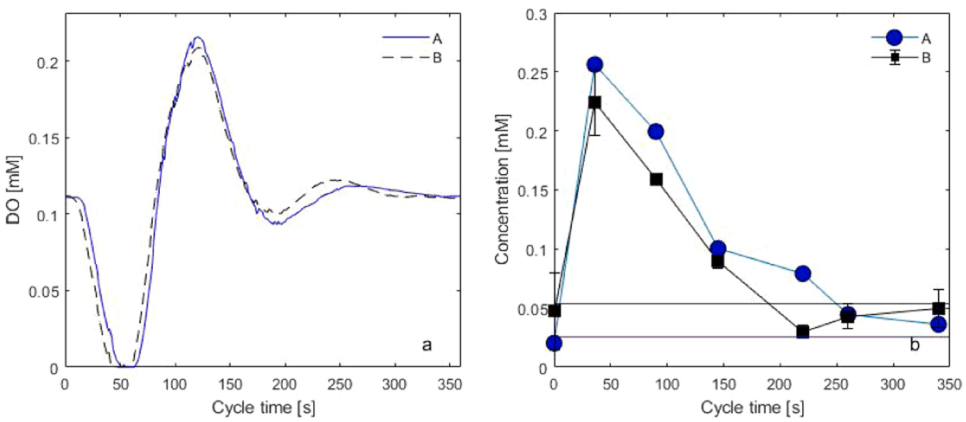

Fig. 1. a) Dissolved oxygen concentration and b) residual glucose concentration during the combined scale down experiment. While experiment A and B are duplicates, in experiment A, the glucose was measured in single samples, while in experiment B duplicates were analyzed. The horizontal lines indicate the concentrations during the steady state phase prior to the oscillation phase. The DO profile presented is corrected for the probe delay. The error bars represent the standard deviation of the measurements.

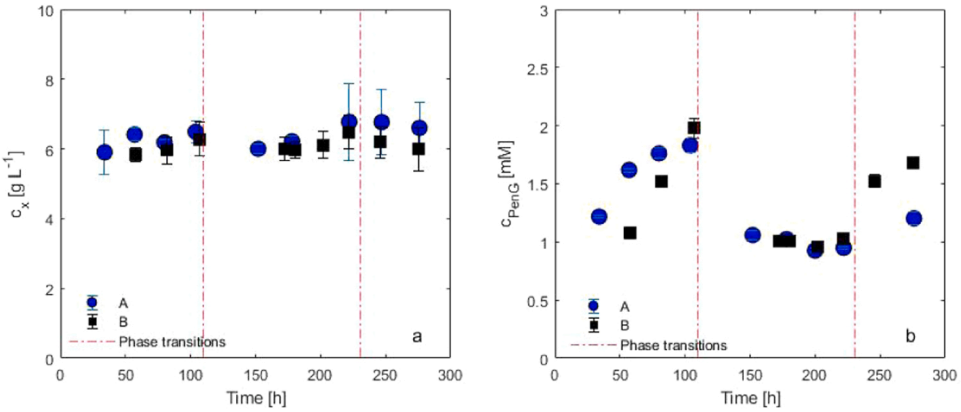

Fig. 2. a) Biomass concentrations, b) penicillin concentrations during the fermentations A and B. The fermentation time of experiment B was shifted 18 h to match the start of the oscillations in the duplicate experiments indicated as A and B.

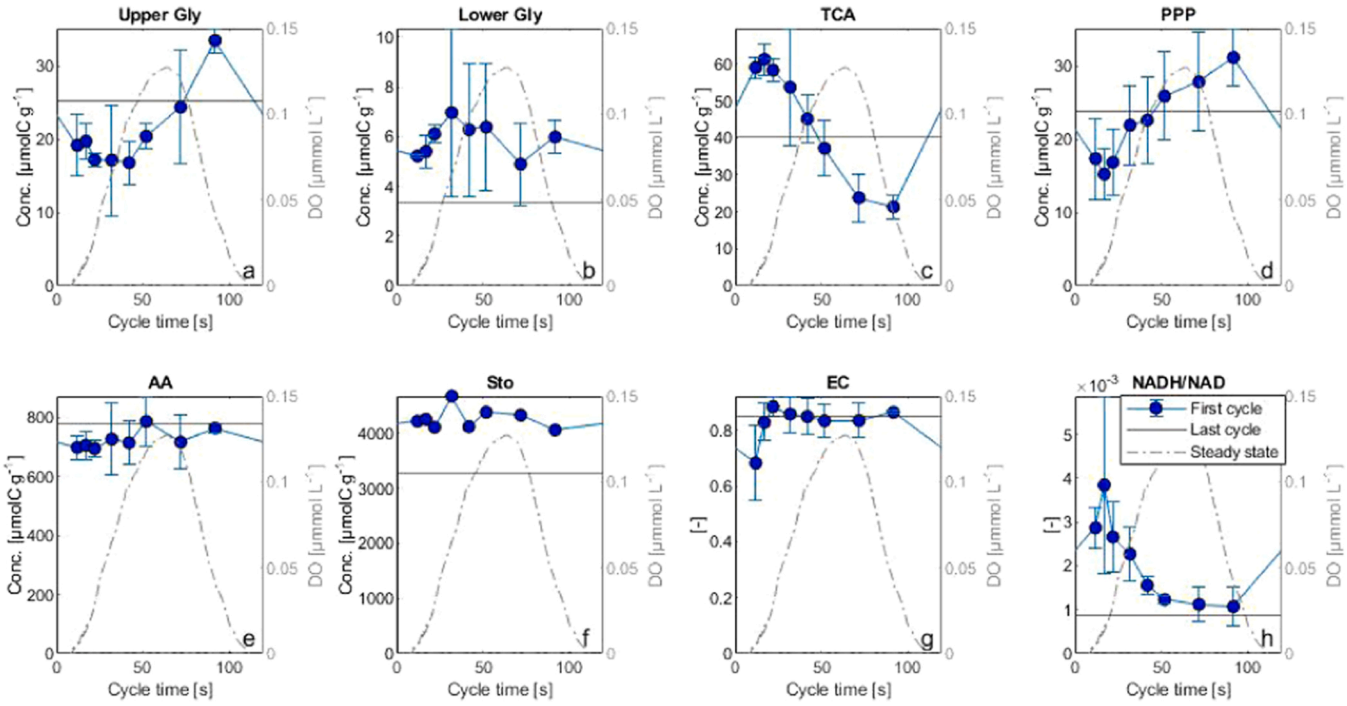

Fig. 3. Metabolite pools in the oxygen oscillation experiment II. For the AA pool, in one of the fermentation αKG was not measured, while in the lower glycolysis pool PEP was not measured. The storage pool is based on the measurements of one fermentation run only as measurements could not be performed on the replicate fermentor.

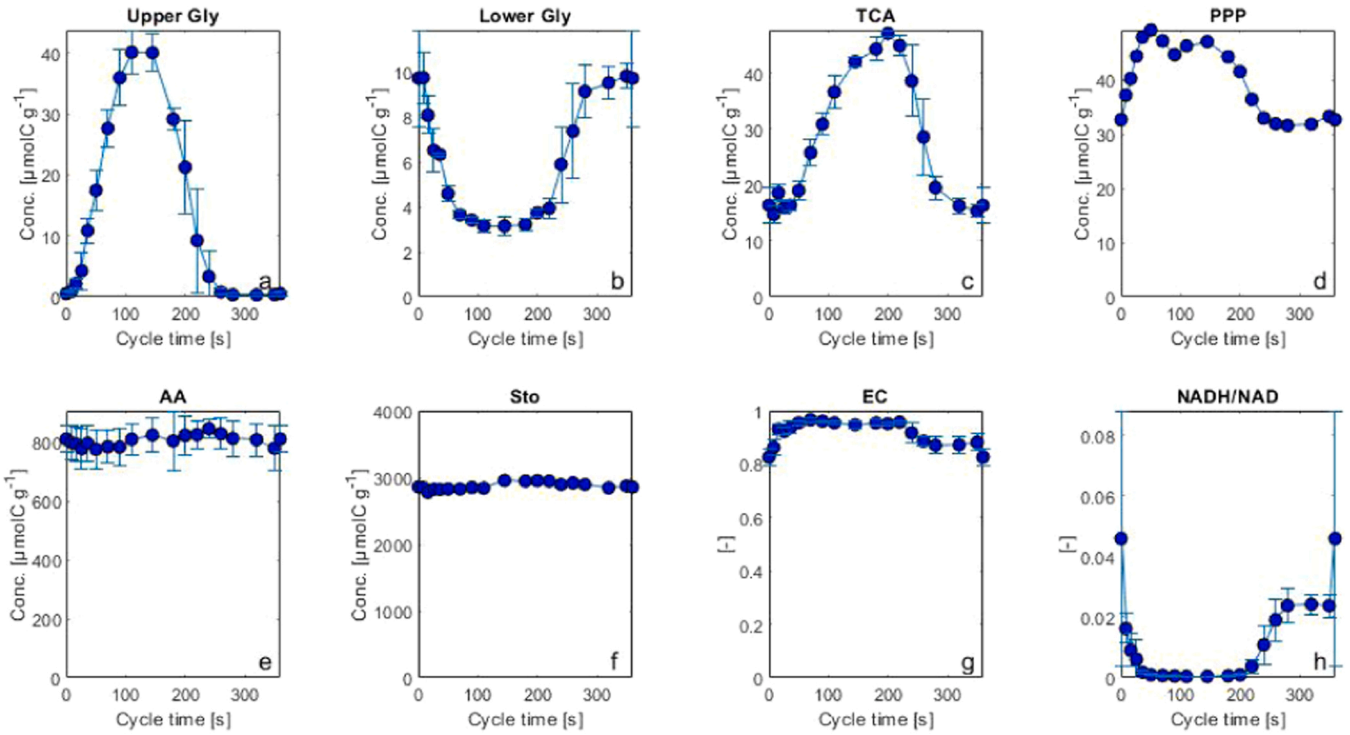

Fig. 4. Glucose oscillation experiments from de Jonge et al. [19]. In TCA intermediates pool, iCit was not measured; in the lower glycolytic intermediates pool DHAP was not measured; in the PPP pool E4P, Ribu5P, Xyl5P was not measured and in the AA pool, Trp was not measured. The PPP and STO intermediates were measured in one of the reactor runs only.

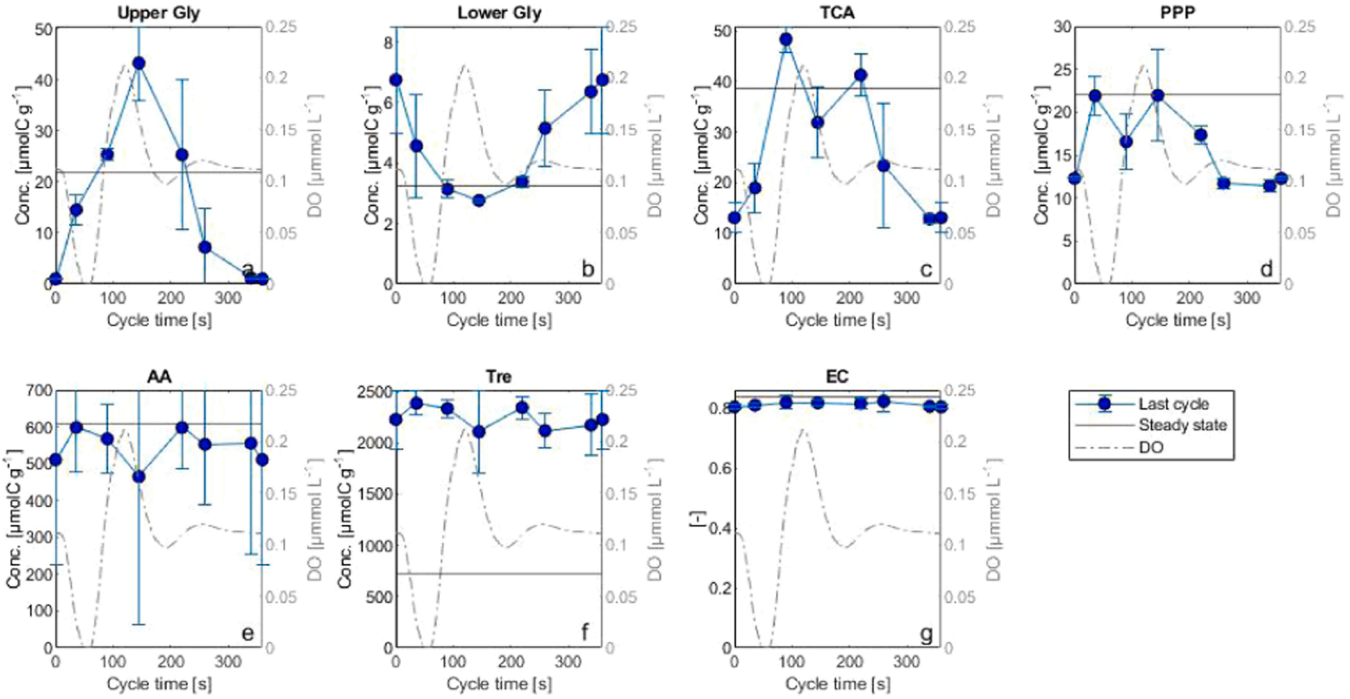

Fig. 5. Metabolite pools in the combined sugar and oxygen oscillation experiment. In the Storage pool only Tre was measured. In the AA pool, Cys could not be detected. The metabolites to calculate the NADH/NAD^+ ratio also could not be measured.

Jonge et al., where 500 rpm was used [19], in a for the rest identical bioreactor. Consequently, a homogenous concentration profile might only take place in the reactor a few seconds after the glucose addition was terminated at 36 s in the cycle. Since the samples were taken less frequently compared to the study of de Jonge, the maximum glucose concentration might not have been identified. The maximum concentration measured at the sampling port at 36 s might therefore not have been a precise representative of the maximum glucose concentration in the reactor in our experiments.

During the initial steady state conditions, the residual glucose

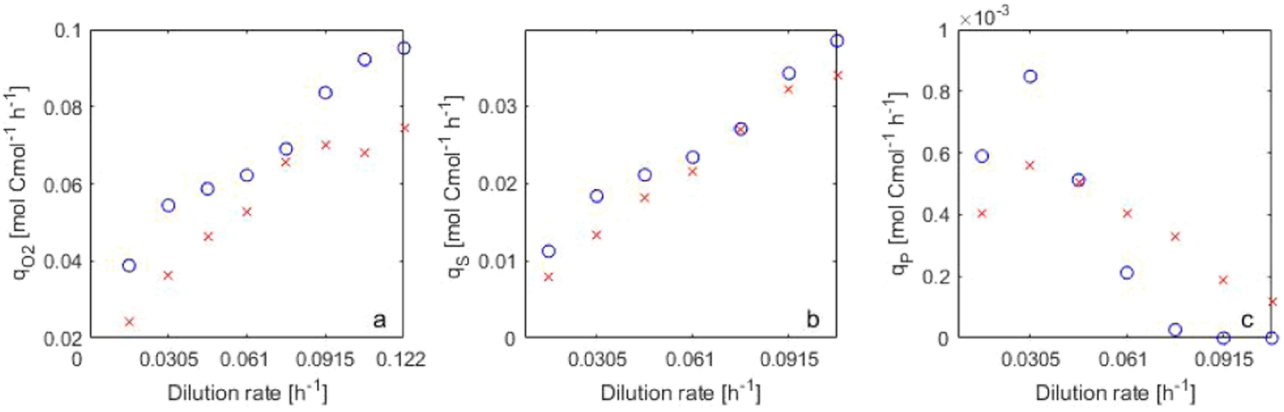

Fig. 6. Steady state experiments at varying dilution rates (7 different experiments with a dilution rate ranging from 0.015 to 0.12 h^{-1}). Red crosses represent the measurements, while the blue circles show the simulations of a) oxygen uptake rate, b) glucose uptake rates and c) penicillin production rates. The q_{CO2} showed similar trends as the q_{O2}, and therefore not presented.

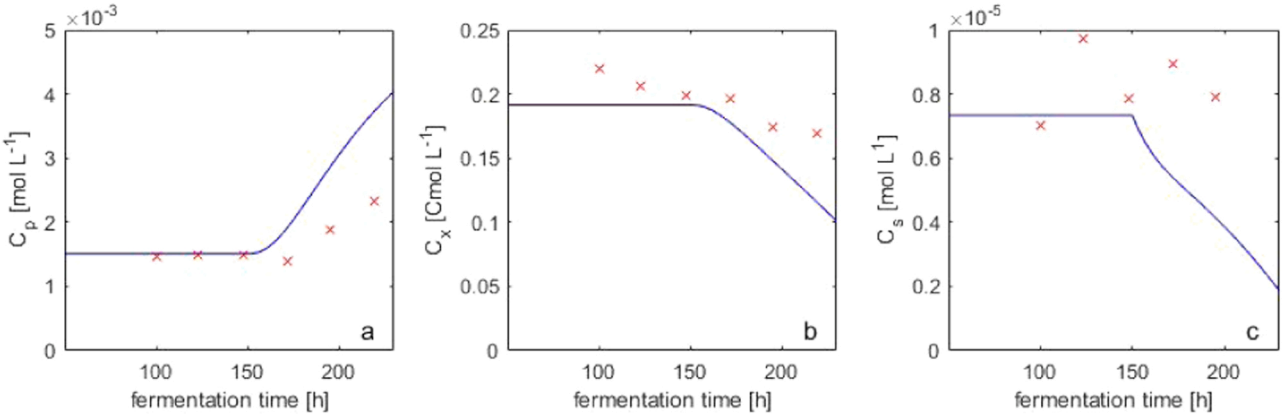

Fig. 7. Ramp experiment (with the dilution rate ranging between 0.5 h-1 −0.05 h-1 between 150 h and 240 h). Red crosses represent the measurements, while the blue line show the simulations of a) penicillin, b) biomass and c) extracellular glucose concentrations.

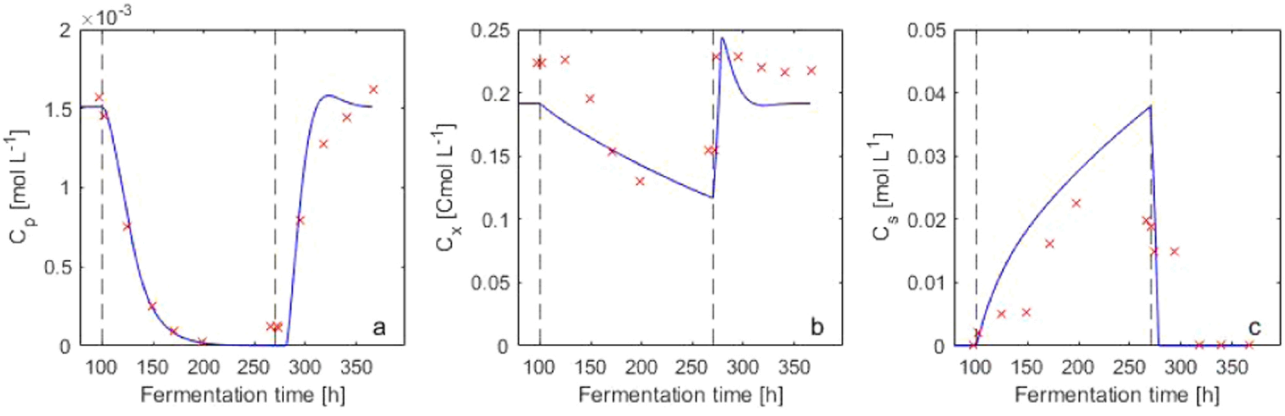

Fig. 8. 0.009 mM DO step experiment. Red crosses represent the measurements, while the blue line show the simulations of a) penicillin, b) biomass and c) extracellular glucose concentrations.

concentration was slightly higher than in the study of Jonge et al. [19], and Wang et al. [28]. Similarly, the glucose concentration did not fall back to zero at the end of the cycle, but remained stable around 0.05 mM, in contrast to previous studies [19,28]. This could indicate that conversion of extracellular trehalose to glucose during the sampling procedure was not completely avoided [19]. Since under similar operational conditions the glucose levels are expected to match, the measurements are expected to be approximately 0.05 mM lower than detected in both experiments. The DO and glucose regimes residence time fractions obtained in the experiments resemble the ones of the large scale reactors, as discussed in the Supplementary material B: experimental design.

3.2. Biomass and penicillin concentrations

The biomass concentration remained stable around 6 ± 0.29 g L^{-1}

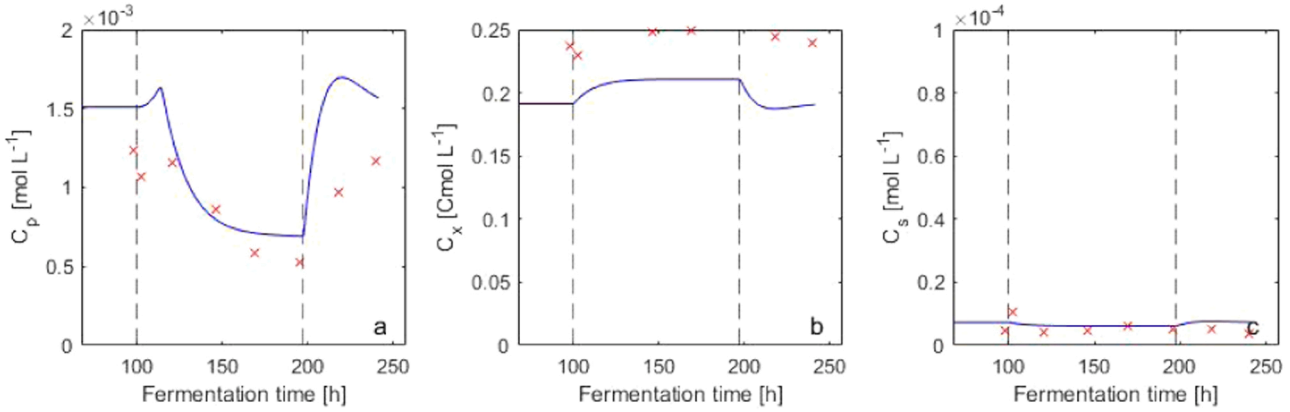

Fig. 9. 0.013 mM DO step experiment. Red crosses represent the measurements, while the blue line show the simulations of a) penicillin, b) biomass and c) extracellular glucose concentrations.

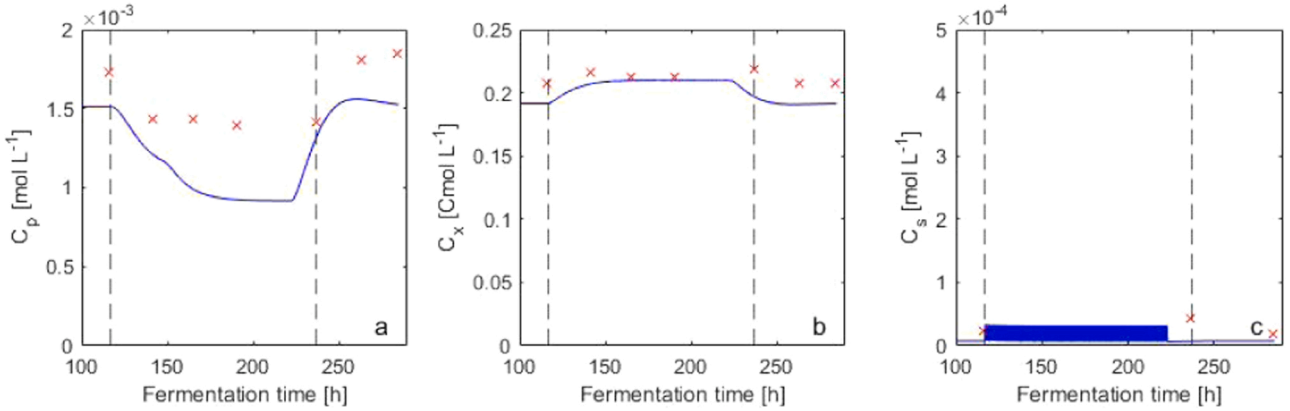

Fig. 10. Oxygen oscillation experiment I. Red crosses represent the measurements, while the blue line show the simulations of a) penicillin, b) biomass and c) extracellular glucose concentrations.

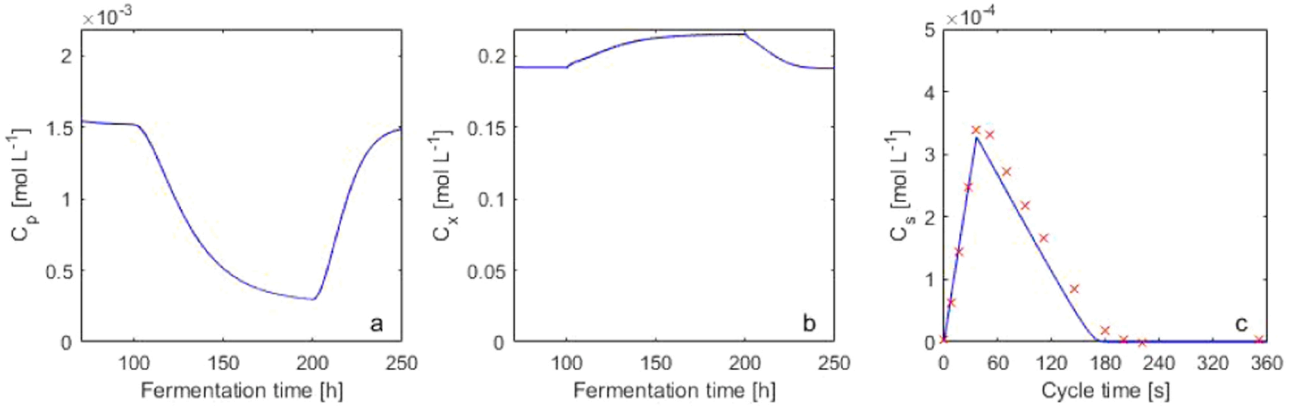

Fig. 11. Glucose oscillation experiment. Red crosses represent the measurements, while the blue line show the simulations of a) penicillin, b) biomass and c) extracellular glucose concentrations. The exact data points of the measurements from this experiments were not available, but presented in the publication of de Jonge et al. [19].

throughout the experiment. This concentration is slightly higher compared to values reported previously for the same dilution rate and medium composition (5.2 ± 0.05 g L^{-1})[19]. The oscillation phase did not significantly affect the biomass concentration in the reactor (Fig. 2a), similarly to previous experiments of separate glucose and oxygen oscillation experiments [5,19]. In contrast to these observations, a slight but significant decline in C_x was observed by Wang et al., under different sugar oscillation regimes [28]. Microscopic analysis did not show any changes in the cellular morphology as a result of the oscillating conditions.

The penicillin concentrations showed a clear increase during the initial chemostat phase, whereby after 100 h both fermentors reached similar concentrations of almost 2 mM, corresponding with a specific penicillin production rate of around 0.0016 mmol g^{-1} h^{-1} (Fig. 2b). These results are matching previous observations [5,19]. During the oscillation phase, the penicillin concentrations of both fermentations

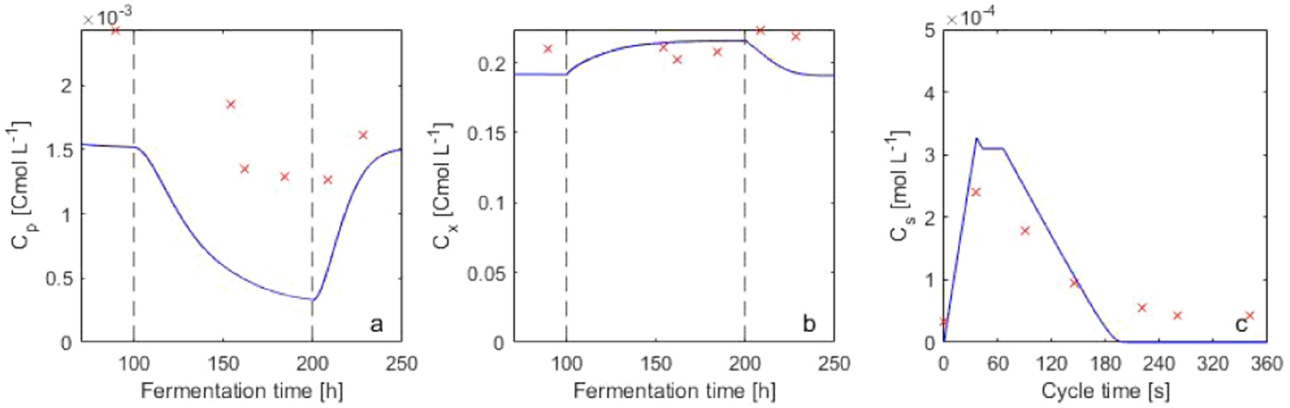

Fig. 12. Combined glucose and oxygen oscillation experiment. Red crosses represent the measurements, while the blue line show the simulations of a) penicillin, b) biomass and c) extracellular glucose concentrations.

declined to 1 mM, corresponding to a specific production rate of approximately 0.007 mmol g^{-1} h^{-1}. The decline in penicillin production rate to approximately 50 % of its original value is similar to that during solely sugar oscillations under otherwise similar conditions. Oscillating oxygen concentrations at constant sugar levels, as introduced in oscillation experiments I and II [5], also resulted in a clear decrease of the specific penicillin production rate, which was approximately 80 % and 50 % in oscillation experiments I and II, respectively. In oscillation experiment I, milder conditions were applied and complete oxygen starvation was maintained for approximately half of the duration of oscillation experiment II (11 s and 23 s below 0.003 mM, respectively). However, in these oxygen oscillation experiments, shorter cycles of approximately 2 min were used, therefore the penicillin production decline was expected to be more intense than in the combined glucose and oxygen oscillation experiments. This is because more frequent limitations were introduced in shorter cycles, because a similar duration of DO starvation was repeated once in 120 s while in the combined experiment this occurred once per 360 s. When comparing the penicillin production rate during the combined oxygen and sugar oscillation experiment to previous experiments of individual glucose or oxygen oscillations, the minor experimental differences such as different stirrer speed and lack of an initial steady-state phase prior to the glucose oscillation experiment, have to be kept in mind. After the initial steady conditions were restored at the end of the experiment, the penicillin production rate partially recovered, similarly to the observations during the separate oxygen oscillation experiments, indicating that the decline of the penicillin production was reversible.

The magnitude of the decline of the penicillin production during the combined scale-down experiment indicates that the combination of the effects of glucose and oxygen fluctuations are not adding up. This might be explained by the fact that the elevated sugar concentrations, which repress expression of the penicillin gene cluster and the low oxygen concentrations, which limit the conversion rate of IPNS, are overlapping and the penicillin production rates therefore do not drop further compared to the individual effects. In case the penicillin gene cluster is repressed, the overall pathway flux might fall below the flux that the IPNS enzyme allows and therefore the total flux won't be influenced by the additional effect of oxygen.

3.3. Comparison of metabolite pools, energy charge and redox state during glucose, oxygen and combined glucose and oxygen scale down experiments

To evaluate the influence of the combined glucose and oxygen gradients on the cellular metabolism, these experiments are compared to separate sugar and oxygen fluctuations or step experiments. In this section, we consider different experiments, such as oxygen step experiments to two different DO values: 0.013 and 0.009 mM, which are discussed in the Supplementary material A: pools and metabolites, oxygen oscillation I and II experiments with differing extent of oxygen starvation within an approximately 2 min cycle [5] and glucose oscillations within 360 s cycles, carried out by de Jonge et al. [19]. The metabolite patterns of certain metabolic pathways, such as the upper and lower glycolysis (Gly), TCA cycle (TCA), pentose phosphate pathway (PPP), amino acids (AA) and storage compounds (Sto) during the single glucose, single oxygen and combined glucose and oxygen oscillation experiments are shown in Figs. 3–5. Additionally, the changes in energy charge (EC) and the redox state ($NADH/NAD^+$) are also plotted.

3.3.1. Oxygen oscillation experiments

On a long term, in the time frame of the fermentation, oscillation experiment I showed a similar response as the step experiments in terms of EC, TCA and PPP intermediates (Supplementary material A: pools and metabolites). On a short term, within the time frame of an oscillation cycle, the redox state and energy charge and consequently also the sizes of the upper and lower glycolytic pools fluctuated, because ATP is required for the phosphorylation steps. Therefore, in the absence of oxygen, the glucose uptake rate had slowed down, affecting the other metabolite groups. Similarly to the step experiments, during oscillation experiment II the upper and lower glycolytic intermediates showed opposite trends. This can be explained by the regulatory mechanism of FBP on the enzyme pyruvate kinase [43]. Therefore, FBP is responsible for the regulation of the transition between the lower glycolysis and the TCA cycle, where a reduced FBP concentration results in lower enzyme rates and therefore might result in accumulation of the lower glycolytic intermediates (See Supplementary material A). The fluctuations in the TCA intermediates are attributed to the fluctuating availability of the NAD^+ cofactor, and the inhibitory effect of NADH on the TCA cycle [44]. Since the upper glycolytic pool is linked to the TCA pool, a delayed response to those can also explain our results.

The pentose phosphate intermediates followed a similar pattern as the upper glycolysis, but with a time delay, possibly due to the conversion from F6P and G6P to PPP intermediates. In oscillation experiment I, where a shorter oxygen starvation period was applied compared to oscillation experiment II, the responses were lacking or were less pronounced and the changes in the lower glycolytic intermediates, EC and $NADH/NAD^+$ could not be observed. The amino acid and storage pools were not influenced within a DO cycle, as the turnover time of these pools are large, and therefore no short term changes could be observed [11].

3.3.2. Sugar oscillation experiments

During the sugar oscillation experiment [19], as a result of feed

supply for 36 s in the 360 s cycle, the extracellular sugar concentration peaked at 36 s and dropped to almost zero around 200 s [19]. The energy charge showed a clear variation, which increased at the beginning of the cycle and stayed at a higher value. The redox state showed similar behaviour as the energy charge, and thereby the NADH/NAD^+ ratio dropped to values approaching 0 between 36 and 200 s in the cycle. However, at high glucose concentrations, the NADH/NAD^+ ratio is expected to increase as a result of an increased rate of glucose dehydrogenation in the glycolysis and TCA cycle and a resulting increased NADH formation [3]. It is therefore possible that the mannitol-1-phosphate dehydrogenase reaction is not quick enough and a fast equilibrium cannot be reached due to a too low activity of this enzyme [2].

The upper glycolytic, TCA and PPP intermediates showed a similar trend as of the extracellular sugar concentration, but with a slight delay, while the lower glycolytic intermediates moved in the opposite direction. In case of a high glycolytic flux the FBP pool increases and pyuvate kinase is activated. Consequently, PEP declines and more PYR is formed and therefore the TCA levels will increase. This explains the correlation between the upper glycolytic intermediates and the TCA cycle intermediates, and the opposing trends between the upper and lower glycolytic intermediates. The declining PEP levels are enhancing this cycle, while further enhancing the phosphofructokinase activity, because phosphofructokinase is inhibited by PEP [45]. The pyruvate concentrations are therefore expected to deviate from the lower glycolytic intermediates, which can be observed from our metabolite measurements (Supplementary Material A and for the glucose oscillation experiments, see [2]). The amino acids and storage compounds were relatively stable, with a slight increase in the middle of the cycle.

3.3.3. Combined oxygen sugar and oxygen oscillations

During the combined oscillation experiment, the energy charge remained stable at a value of 0.8. Since during the individual sugar or oxygen oscillations, the energy charge showed fluctuations, it is possible therefore that the effect of declining oxygen and the increasing glucose concentration have balanced each other. The upper glycolytic intermediates showed an increase at the beginning of the cycle, while the lower glycolytic intermediates decreased. This is similar as observed in the oscillating sugar experiments [19], and it might be explained by the activation of pyruvate kinase by FBP at high glucose levels. The upper glycolytic intermediates followed the observed trend in the extracellular glucose concentration, but a delayed response was observed. According to the oxygen oscillation experiment, at low oxygen levels in a cycle, the upper glycolytic pool is expected to drop but this pattern was not observed in the measurements. The range of the glycolytic intermediate variations were identical in the oxygen and glucose oscillations and in the glucose oscillations alone, however, the upper glycolytic intermediates did not decline as quick as in the case of only sugar oscillations. This is possibly due to their slower conversion to other metabolites in the absence of oxygen, and thus in a slower depletion rate of this pool.

The TCA cycle intermediates accumulated in the first part of the cycle and reached their maximum at 90 s, which was followed by a temporary drop at 145 s and increased again until 220 s before the concentration declined until the end of the cycle. This dip in the concentration profile was not observed in previous sugar oscillation experiments [19,28,46], and can be attributed to the influence of oxygen. In the absence of oxygen, the decline in NAD^+ concentration might result in a decrease of the TCA cycle flux and the depletion of TCA intermediates. However, the errors related to this single measurement point might question the significance of this dip. The average pool size of the TCA intermediates was lower compared to the steady state values, which was observed previously in feast famine cycles and was attributed to adaptation of the cells to the quickly changing conditions and facilitating to cope with the rapidly changing substrate availability by maintaining pools with faster turnover [47].

The pentose phosphate intermediates showed accumulation between 0 and 90 s in the cycle, similarly to solely glucose oscillation experiments [19]. This is possibly due the direct linkage of the PPP pool to the upper glycolytic pool. However, a dip in the concentration of the PPP intermediates at 90 s might be related to a reduced oxygen availability, and a temporary drop in the ATP pool, re-arranging the carbon flux towards the PPP. However, this dip is not statistically significant. Towards the end of the cycle, the PPP intermediates have declined.Similarly to the individual oxygen or glucose oscillation experiments, the amino acid and storage pools did not show dynamics in a cycle, which is related to their long turnover times.

Generally, the additional effect of oxygen oscillation next to the glucose oscillation cycles was not observable in most metabolite pools. During the reduced oxygen availability, reduced ATP and NAD^+ cofactors are available, influencing the rate of many metabolic processes as shown in the oxygen oscillation experiments. However, due to the alternating oxygen availability in the combined oscillation experiments, the influence of fluctuations of these molecules might be hidden behind the influence of the glucose pulses on the central metabolism, redox state and ATP availability. The lack of influence of the fluctuating oxygen concentrations next to the fluctuating sugar concentrations is also reflected in the extracellular penicillin and glucose concentration measurements.

3.4. Model simulations

Regarding glucose limited chemostat experiments at different dilution rates, the model gave good predictions of the trends of the experimentally observed q_{O2}, q_{CO2}, q_S and q_P during steady state, and also of the C_p, C_x and C_s in the ramp experiment (Figs. 6 and 7). The model predicted the trends of increasing O_2 uptake, CO_2 production and sugar uptake with increased dilution rate. The penicillin production rate and the penicillin concentrations showed a maximum at a dilution of 0.03 h^{-1}, in good correlation with experimental data [35]. This is possibly reasoned by the repression of the gene cluster by extracellular glucose, taking place at dilution rates exceeding 0.03 h^{-1} [26]. Additionally, during the ramp experiment, the trends of the intracellular metabolite pools were well captured in the model, although the X_{GLY} pool size was under predicted (Appendix, Figure A2).

Regarding the DO step experiments, the model predicted the C_x, C_s and C_p profiles in the experiments well (Figs. 8 and 9). The declining trend in the penicillin concentration at low DO was also well predicted. This was due to the low oxygen levels influencing the IPN synthesis rate, resulting in a declining IPN pool size which negatively influenced the penicillin synthesis rate. Additionally, in the 0.009 mM step experiment, the increasing extracellular glucose concentration might have repressed the penicillin gene cluster, further contributing to the reduced penicillin synthesis rate. The intracellular pools related to these experiments (X_{GLY}, X_{STO} and X_{ATP}, Appendix, Figure A3 and A4) did not show changes according to the predictions, similarly to the experimental data which also didn't show clear changes. The decline in the biomass growth rate was attributed to the decline in the NAD^+ concentration in the model.

The oxygen oscillation experiments and the combined oxygen and glucose scale-down experiments were only used for model validation. In the oxygen oscillation experiment I, the experimentally observed slight increase in biomass concentration and the decline in penicillin concentration was captured well (Fig. 10). The penicillin production rate did not show large fluctuations, because the oxygen level affected the IPN pool directly and the penicillin production rate therefore decreased to a steady reduced level. The levels of the glycolytic intermediates in this experiment followed the same trend as the measurements, while the ATP concentration showed a larger drop in the simulations than in our measurements and decreased to zero in the absence of oxygen (Fig. A5, Appendix). This is most probably caused by cellular regulation, whereby the ATP level is tightly controlled to achieve ATP homoeostasis [48,49], which was not included in the model. Due to the periodical small extracellular glucose increase, the predicted concentration of the

enzyme pool related to the penicillin synthesis dropped slightly.

During the sugar oscillation experiment the predictions were good in terms of predicting the dynamic changes within a cycle regarding C_s (Fig. 11), and X_{ATP}, X_{STO}, and X_{GLY}, however, the X_{GLY} pool size was under predicted (Figure A6, Appendix). On a long term during the sugar oscillations, the declining trend in penicillin concentration was represented by the model, however, the extent of the penicillin concentration decline was overestimated. The penicillin concentration declined to 20 % of its value after 100 h of sugar oscillations according to the prediction, while in the measurements of Jonge et al., it was only approximately 50 % [19]. The penicillin concentration decline is reasoned in the model by the periodic glucose starvation, limiting the penicillin synthesis and glucose excess conditions which represses the gene cluster. Because the penicillin concentration in this experiment was not used in the parameter estimation procedure, and its solely based on predictions from parameters fitted using data from other experiments, it's possible that predictions at such extreme glucose concentrations are not captured well in the model. The exaggerated penicillin production decline could be further improved by applying the measured penicillin concentrations for the parameter fitting. The biomass concentration showed a slight elevation in the predictions during the fermentation (7 %), which might not be easily observable in the experimental measurements.

In the combined glucose and oxygen oscillation experiment, the penicillin concentration drop was overestimated, similarly as for the glucose oscillation experiments. The extent of the drop was the same as during the individual feast famine cycles, indicating that no additional effect of oxygen oscillations takes place, resembling the experimental observations. During the cycle, the expected C_s was well approximated and the X_{GLY} was under predicted (Figure A7, Appendix). Similarly to the oxygen oscillation experiments, the drop in the ATP concentration at the time moments when the DO dropped to zero were overestimated, and ATP levels of zero were noted. Generally, the trends of all the measured intracellular pools were captured well in the model, but the exact values showed slight alternation. Evaluating the relative errors between the predictions and the measurements shows that when averaging the errors of the pools and time points, the metabolite trends of each experiment are predicted with a 31 % error. There was no difference between the errors in the experiments which were used for the model parameter fitting and those which were predicted, showing the reliability of the model. Amongst the pools, the glycolytic pool and the extracellular glucose pool showed the largest deviations from the measurements, while the biomass concentration, the storage compounds and the ATP pool are predicted relatively well with an average relative error $<$11 %.

The model simulations predicted the trends in biomass growth and penicillin production by considering the influence of the relevant intracellular pools and metabolic processes, however, the model has several limitations and can be further improved. The largest challenge of the pooled modelling approach is the large number of unknown parameters which are making the parameter estimation challenging. In the presented model, not all model parameters could be well defined, because the measured pool sizes in this study are not sufficient to clearly define all the model parameters. Non-identifiably is a common problem with metabolic models [9], although predictions with non-identifiable parameter values still can lead to useful models with good predictions [50]. Well-designed experiments and targeted omics measurements could bring further understanding of the pathway regulations, resulting in an improved model structure. As obtaining more detailed experimental data is laborious, the model could be further simplified to reduce the number of unknown parameters. Kinetic terms which do not show strong involvement could therefore be eliminated or variables could be pooled further to reduce the model [12]. Although we have applied metabolite lumping and eliminated several pools from a previous model [11], the model network and structure could be further simplified. Drawing biological conclusions about control mechanisms from the model is not straightforward, as parameter sensitivities are difficult to obtain [51], which makes it difficult to predict from which biological modification the penicillin production could benefit the most. For future work, model improvements are recommended based on network structures, model reduction, more accurate kinetic terms and parameter values [9,51].

On the other hand, the model presents good predictions of the observed trends of C_p, C_x and C_s under dynamic conditions on time scales of seconds to minutes and fluctuations in both glucose and oxygen levels, as validated by 2 experiments. Compared to the black box model, good predictions for the trends of the penicillin concentrations are available. According to simulations with the black box model under feast famine conditions, no penicillin production takes place as presented in the study of Tang et al.[11]. The black box model lacks dynamics and intermediate metabolite pools (such as storage or IPN pool) and therefore negative growth and penicillin production rates are achieved under glucose starvation. Therefore, the presented dynamic modelling approach is advantageous and is strongly recommended for application in coupled CFD models to describe productivity under heterogeneous substrate and DO availability. With the help of the coupled CFD-kinetic model predictions, further improvements on the process can be achieved, such as sparger design or feeding port locations [7].

4. Conclusions

To obtain accurate predictions of large scale penicillin fermentations, heterogeneities in terms of oxygen and glucose in industrial scale fermentors have to be considered. This study aimed to design scale down experiments based on lifeline data obtained from CFD simulations of large scale fermentors. Additionally, we developed a metabolic structured kinetic model describing the cellular responses to a dynamically changing environment. Metabolite pools obtained from chemostat experiments at varying dilution rates and oxygen levels, next to cycling feast famine experiments, were used for parameter estimation of the model. The obtained metabolite pools of the scale-down experiment of solely oxygen and combined glucose and oxygen oscillation experiments were used for model validation.

The scale down experiments designed in this study represented the total residence time fractions obtained from the CFD simulations of the large scale tanks well, while compromising on the time periods the cells reside in a certain regime. Metabolite analysis of the scale-down experiments wherein combined oxygen and glucose oscillations were achieved, showed that measured metabolite pools, i.e. amino acids, upper and lower glycolytic intermediates, TCA cycle intermediates and pentose phosphate cycle intermediates, closely resembled what was observed in the glucose oscillation experiments, showing little influence of the additional oxygen oscillations. Similarly, the decline of penicillin production also resembled the glucose oscillations only without an additional effect of the oxygen.

The developed metabolic structured kinetic model was able to adequately predict extracellular concentrations of glucose, biomass and penicillin, next to intracellular metabolite pool concentrations. Simulations under dynamic conditions resulted in predictions of the metabolite pools on a seconds scale and predicted changes in the penicillin and biomass concentration on the time scale of a fermentation. Despite some discrepancies between model predictions and simulations, the trends of both extra and intracellular metabolite pools were well predicted under both glucose, oxygen and combined glucose and oxygen gradients, where the latter two served for model validation. Coupling the developed kinetic model to CFD simulations should provide improved lifeline data to guide further scale down experiments aimed at improving the performance of large scale fermentations through improvement of the producing strain and/or the operating conditions of the bioreactor.

Funding

This project is supported by ERA CoBioTech/EU H2020 project

(grant 722361) “ComRaDes”, a public–private partnership between the University of Stuttgart, TU Delft, University of Liege, DSM, Centrient Pharmaceuticals and Syngulon.

Associated content

Supporting Information (Supplementary material A and B) Appendix.

Declaration of Competing Interest

This project is sponsored by Centrient Pharmaceuticals a producer of lactam antibiotics, and DSM a global company active in Nutrition, Health & Sustainable Living.

Data availability

The authors are unable or have chosen not to specify which data has been used.

Acknowledgements

Thanks to Jelle J. Verheijen, Wenjung Tang, Anne Hensen and Queenie Lee for their contribution to the experimental work related to the oxygen oscillation and step experiments. Additionally, thanks to Wenjung Tang for his insights regarding model development.

Appendix A. Supporting information

Supplementary data associated with this article can be found in the online version at doi:10.1016/j.procbio.2022.11.006.

References

[1] M. Kuschel, R. Takors, Simulated oxygen and glucose gradients as a prerequisite for predicting industrial scale performance a priori, Biotechnol. Bioeng. (2020).
[2] L.P. de Jonge, A scale-down study of the industrial penicillin fermentation using quantitative metabolomics, Neth. Delft Univ. Technol. 192 (2016).
[3] C.A. Suarez-Mendez, A. Sousa, J.J. Heijnen, A. Wahl, Fast “feast/famine” cycles for studying microbial physiology under dynamic conditions: a case study with Saccharomyces cerevisiae, Metabolites 4 (2014) 347–372.
[4] B. Lorantfy, M. Jazini, C. Herwig, Investigation of the physiological response to oxygen limited process conditions of Pichia pastoris Mut+ strain using a two-compartment scale-down system, J. Biosci. Bioeng. 116 (2013) 371–379.
[5] A. Janoska, J.J. Verheijen, W. Tang, Q. Lee, B. Sikkema, W.M. van Gulik, Influence of oxygen concentration on the metabolism of Penicillium chrysogenum, Eng. Life Sci. (2022).
[6] C. Haringa, W. Tang, A.T. Deshmukh, J. Xia, M. Reuss, J.J. Heijnen, R.F. Mudde, H. J. Noorman, Euler-lagrange computational fluid dynamics for (bio) reactor scale down: an analysis of organism lifelines, Eng. Life Sci. 16 (2016) 652–663.
[7] G. Wang, W. Tang, J. Xia, J. Chu, H. Noorman, W.M. van Gulik, Integration of microbial kinetics and fluid dynamics toward model-driven scale-up of industrial bioprocesses, Eng. Life Sci. 15 (2015) 20–29.
[8] A. Lapin, D. Müller, M. Reuss, Dynamic behavior of microbial populations in stirred bioreactors simulated with Euler− Lagrange methods: Traveling along the lifelines of single cells, Ind. Eng. Chem. Res. 43 (2004) 4647–4656.
[9] E. Vasilakou, D. Machado, A. Theorell, I. Rocha, K. Nöh, M. Oldiges, S.A. Wahl, Current state and challenges for dynamic metabolic modeling, Curr. Opin. Microbiol. 33 (2016) 97–104.
[10] G. Wang, C. Haringa, H. Noorman, J. Chu, Y. Zhuang, Developing a computational framework to advance bioprocess scale-up, Trends Biotechnol. (2020).
[11] W. Tang, A.T. Deshmukh, C. Haringa, G. Wang, W. van Gulik, W. van Winden, M. Reuss, J.J. Heijnen, J. Xia, J. Chu, A 9–pool metabolic structured kinetic model describing days to seconds dynamics of growth and product formation by Penicillium chrysogenum, Biotechnol. Bioeng. 114 (2017) 1733–1743.
[12] S. Danø, M.F. Madsen, H. Schmidt, G. Cedersund, Reduction of a biochemical model with preservation of its basic dynamic properties, FEBS J. 273 (2006) 4862–4877.
[13] A.R. Lara, E. Galindo, O.T. Ramírez, L.A. Palomares, Living with heterogeneities in bioreactors, Mol. Biotechnol. 34 (2006) 355–381.
[14] C. Haringa, A.T. Deshmukh, R.F. Mudde, H.J. Noorman, Euler-Lagrange analysis towards representative down-scaling of a 22 m3 aerobic S. cerevisiae fermentation, Chem. Eng. Sci. 170 (2017) 653–669.
[15] A. Lapin, J. Schmid, M. Reuss, Modeling the dynamics of E. coli populations in the three-dimensional turbulent field of a stirred-tank bioreactor—a structured–segregated approach, Chem. Eng. Sci. 61 (2006) 4783–4797.
[16] D. Vlaev, R. Mann, V. Lossev, S.D. Vlaev, J. Zahradnik, P. Seichter, Macro-mixing and Streptomyces fradiae: modelling oxygen and nutrient segregation in an industrial bioreactor, Chem. Eng. Res. Des. 78 (2000) 354–362.
[17] H. Hristov, R. Mann, V. Lossev, S.D. Vlaev, P. Seichter, A 3-D analysis of gas-liquid mixing, mass transfer and bioreaction in a stirred bio-reactor, Food Bioprod. Process. 79 (2001) 232–241.
[18] T.K. Villiger, B. Neunstoecklin, D.J. Karst, E. Lucas, M. Stettler, H. Broly, M. Morbidelli, M. Soos, Experimental and CFD physical characterization of animal cell bioreactors: from micro-to production scale, Biochem. Eng. J. 131 (2018) 84–94.
[19] L.P. de Jonge, N.A.A. Buijs, A. ten Pierick, A. Deshmukh, Z. Zhao, J.A.K.W. Kiel, J. J. Heijnen, W.M. van Gulik, Scale-down of penicillin production in Penicillium chrysogenum, Biotechnol. J. 6 (2011) 944–958.
[20] E. Vasilakou, M.C.M. Van Loosdrecht, S.A. Wahl, Escherichia coli metabolism under short-term repetitive substrate dynamics: adaptation and trade-offs, Microb. Cell Fact. 19 (2020) 1–19.
[21] F. Vardar, M.D. Lilly, Effect of cycling dissolved oxygen concentrations on product formation in penicillin fermentations, Eur. J. Appl. Microbiol. Biotechnol. 14 (1982) 203–211.
[22] E.A. Sandoval-Basurto, G. Gosset, F. Bolívar, O.T. Ramírez, Culture of Escherichia coli under dissolved oxygen gradients simulated in a two-compartment scale-down system: metabolic response and production of recombinant protein, Biotechnol. Bioeng. 89 (2005) 453–463.
[23] V. Cappello, C. Plais, C. Vial, F. Augier, Scale-up of aerated bioreactors: CFD validation and application to the enzyme production by Trichoderma reesei, Chem. Eng. Sci. 229 (2021), 116033.
[24] C.J. Hewitt, G. Nebe-Von Caron, B. Axelsson, C.M. McFarlane, A.W. Nienow, Studies related to the scale-up of high-cell-density E. coli fed-batch fermentations using multiparameter flow cytometry: effect of a changing microenvironment with respect to glucose and dissolved oxygen concentration, Biotechnol. Bioeng. 70 (2000) 381–390.
[25] Á.C. García, P. Hauptmann, P. Neubauer, Glucose-limited fed-batch cultivation strategy to mimic large-scale effects in Escherichia coli linked to accumulation of non-canonical branched-chain amino acids by combination of pyruvate pulses and dissolved oxygen limitation, Microorganisms 9 (2021) 1110.
[26] R.D. Douma, P.J.T. Verheijen, W.T.A.M. de Laat, J.J. Heijnen, W.M. van Gulik, Dynamic gene expression regulation model for growth and penicillin production in Penicillium chrysogenum, Biotechnol. Bioeng. 106 (2010) 608–618.
[27] H.B.A. Theilgaard, K.N. Kristiansen, C.M. Henriksen, J. Nielsen, Purification and characterization of δ-(L-α-aminoadipyl)-L-cysteinyl-D-valine synthetase from Penicillium chrysogenum, Biochem. J. 327 (1997) 185–191.
[28] G. Wang, J. Zhao, C. Haringa, W. Tang, J. Xia, J. Chu, Y. Zhuang, S. Zhang, A. T. Deshmukh, W. van Gulik, Comparative performance of different scale-down simulators of substrate gradients in Penicillium chrysogenum cultures: the need of a biological systems response analysis, Microb. Biotechnol. 11 (2018) 486–497.
[29] S. Niedenführ, A. ten Pierick, P.T.N. van Dam, C.A. Suarez-Mendez, K. Nöh, S. A. Wahl, Natural isotope correction of MS/MS measurements for metabolomics and 13C fluxomics, Biotechnol. Bioeng. 113 (2016) 1137–1147.
[30] D. Visser, G.A. van Zuylen, J.C. van Dam, M.R. Eman, A. Pröll, C. Ras, L. Wu, W. M. van Gulik, J.J. Heijnen, Analysis of in vivo kinetics of glycolysis in aerobic Saccharomyces cerevisiae by application of glucose and ethanol pulses, Biotechnol. Bioeng. 88 (2004) 157–167.
[31] T. Nemkov, K.C. Hansen, A. D'Alessandro, A three-minute method for high-throughput quantitative metabolomics and quantitative tracing experiments of central carbon and nitrogen pathways, Rapid Commun. Mass Spectrom. 31 (2017) 663–673.
[32] R.M. Seifar, C. Ras, J.C. van Dam, W.M. van Gulik, J.J. Heijnen, W.A. van Winden, Simultaneous quantification of free nucleotides in complex biological samples using ion pair reversed phase liquid chromatography isotope dilution tandem mass spectrometry, Anal. Biochem. 388 (2009) 213–219.
[33] A.B. Canelas, C. Ras, A. ten Pierick, W.M. van Gulik, J.J. Heijnen, An in vivo data-driven framework for classification and quantification of enzyme kinetics and determination of apparent thermodynamic data, Metab. Eng. 13 (2011) 294–306.
[34] A.B. Canelas, W.M. van Gulik, J.J. Heijnen, Determination of the cytosolic free NAD/NADH ratio in Saccharomyces cerevisiae under steady-state and highly dynamic conditions, Biotechnol. Bioeng. 100 (2008) 734–743.
[35] W.M. Van Gulik, W. De Laat, J.L. Vinke, J.J. Heijnen, Application of metabolic flux analysis for the identification of metabolic bottlenecks in the biosynthesis of penicillin-G, Biotechnol. Bioeng. 68 (2000) 602–618.
[36] E. Balsa-Canto, D. Henriques, A. Gábor, J.R. Banga, AMIGO2, a toolbox for dynamic modeling, optimization and control in systems biology, Bioinformatics 32 (2016) 3357–3359.
[37] J.A. Egea, E. Balsa-Canto, M.-S.G. Garcia, J.R. Banga, Dynamic optimization of nonlinear processes with an enhanced scatter search method, Ind. Eng. Chem. Res. 48 (2009) 4388–4401.
[38] J.A. Egea, M. Rodríguez-Fernández, J.R. Banga, R. Martí, Scatter search for chemical and bio-process optimization, J. Glob. Optim. 37 (2007) 481–503.
[39] E. Walter, L. Pronzato, Identification of parametric models, Commun. Control Eng. 8 (1997).
[40] E. Balsa-Canto, J.R. Banga, AMIGO: a model identification toolbox based on global optimization and its applications in biosystems, IFAC Proc. 43 (2010) 132–137.
[41] A.G. and J.R.B. Eva Balsa-Canto, David Henriques, AMIGO2, Theoretical background, (2016) 1–27. https://sites.google.com/site/amigo2toolbox/doc (accessed February 21, 2021).

[42] C.M. Henriksen, J. Nielsen, J. Villadsen, Influence of the dissolved oxygen concentration on the penicillin biosynthetic pathway in steady-state cultures of Penicillium chrysogenum, Biotechnol. Prog. 13 (1997) 776–782.
[43] M.S. Jurica, A. Mesecar, P.J. Heath, W. Shi, T. Nowak, B.L. Stoddard, The allosteric regulation of pyruvate kinase by fructose-1, 6-bisphosphate, Structure 6 (1998) 195–210.
[44] C.P. Kubicek, Regulatory aspects of the tricarboxylic acid cycle in filamentous fungi—a review, Trans. Br. Mycol. Soc. 90 (1988) 339–349.
[45] D. Buckwitz, G. Jacobasch, C. Gerth, Phosphofructokinase from Plasmodium berghei: a kinetic model of allosteric regulation, Mol. Biochem. Parasitol. 40 (1990) 225–232.
[46] G. Wang, J. Chu, Y. Zhuang, W. van Gulik, H. Noorman, A dynamic model-based preparation of uniformly-13C-labeled internal standards facilitates quantitative metabolomics analysis of Penicillium chrysogenum, J. Biotechnol. 299 (2019) 21–31.
[47] X. Wang, J. Zhao, J. Xia, G. Wang, J. Chu, Y. Zhuang, Impact of altered trehalose metabolism on physiological response of penicillium chrysogenum chemostat cultures during industrially relevant rapid feast/famine conditions, Processes 9 (2021) 118.
[48] G. Giordano, L.M. de Graaf, E. Vasilakou, S.A. Wahl, Unraveling energy homeostasis in a dynamic model of glycolysis in Escherichia coli, in: 2019 18th Eur. Control Conf., IEEE, 2019: pp. 2140–2145.
[49] F. Hillmann, E. Shekhova, O. Kniemeyer, Insights into the cellular responses to hypoxia in filamentous fungi, Curr. Genet. 61 (2015) 441–455.
[50] S. van Mourik, C. Ter Braak, H. Stigter, J. Molenaar, Prediction uncertainty assessment of a systems biology model requires a sample of the full probability distribution of its parameters, PeerJ 2 (2014), e433.
[51] J. Almquist, M. Cvijovic, V. Hatzimanikatis, J. Nielsen, M. Jirstrand, Kinetic models in industrial biotechnology–improving cell factory performance, Metab. Eng. 24 (2014) 38–60.